Automated 3D Whole-Heart Mesh Reconstruction From 2D Cine MR Slices Using Statistical Shape Model*

Abhirup Banerjee[1], Ernesto Zacur[2], Robin P. Choudhury[3] and Vicente Grau[2]

***Abstract*— Cardiac magnetic resonance (CMR) imaging is the one of the gold standard imaging modalities for the diagnosis and characterization of cardiovascular diseases. The clinical cine protocol of the CMR typically generates high-resolution 2D images of heart tissues in a finite number of separated and independent 2D planes, which are appropriate for the 3D reconstruction of biventricular heart surfaces. However, they are usually inadequate for the whole-heart reconstruction, specifically for both atria. In this regard, the paper presents a novel approach for automated patient-specific 3D whole-heart mesh reconstruction from limited number of 2D cine CMR slices with the help of a statistical shape model (SSM). After extracting the heart contours from 2D cine slices, the SSM is first optimally fitted over the sparse heart contours in 3D space to provide the initial representation of the 3D whole-heart mesh, which is further deformed to minimize the distance from the heart contours for generating the final reconstructed mesh. The reconstruction performance of the proposed approach is evaluated on a cohort of 30 subjects randomly selected from the UK Biobank study, demonstrating the generation of high-quality 3D whole-heart meshes with average contours to surface distance less than the underlying image resolution and the clinical metrics within acceptable ranges reported in previous literature.**

***Clinical relevance*— Automated patient-specific 3D whole-heart mesh reconstruction has numerous applications in cardiac diagnosis and multimodal visualization, including treatment planning, virtual surgery, and biomedical simulations.**

***Index Terms*— 3D cardiac mesh reconstruction, Whole heart reconstruction, Cine MRI, Biatrial reconstruction, Statistical shape model.**

I. INTRODUCTION

Cardiac magnetic resonance (CMR) imaging is one of the gold standard medical imaging modalities for providing both anatomical and functional information of the heart. Due to its ability to characterize soft tissues non-invasively without using any ionizing radiation, CMR has gained popularity for evaluating the myocardium, specifically for the accurate assessments of left ventricular (LV) function, myocardial perfusion, oedema, and scar [1]. In common clinical applications, the cine CMR protocol typically images the heart structure in a finite number of image planes with good contrast between soft tissues at a reasonable temporal resolution, with an about 1.5×1.5 mm^2 in-plane resolution and $8 - 10$ mm out-of-plane resolution. Although the 2D CMR images can reveal the presence of scar or oedema, myocardial perfusion, microvascular obstruction, etc. on heart tissues, their accurate localization on the 3D heart model can enable the clinicians to understand their shapes and relationship with the surrounding anatomy. Heart shapes have been shown to provide improved diagnosis and prognosis in clinical applications, thus necessitating the development of automated patient-specific 3D cardiac mesh reconstruction from finite number of acquired 2D cine CMR images.

Although significant number of research works have been performed on the reconstruction of 3D surfaces from 2D images [2], [3], [4], a limited number of methods has been applied on 3D heart meshes, specifically from a finite number of sparse 2D cine CMR slices. Given a set of sparse contours or delineated curves on 2D heart slices, some methods have attempted to reconstruct the 3D heart surfaces using manifold interpolating surface [5], cubic periodic B-splines [6], [7], curve networks of arbitrary shape and topology on cross-section planes [3], etc. Integrating the cine MR slices selection, segmentation, misalignment correction, and mesh surface reconstruction into a completely automated pipeline, a method has been recently developed for generating patient-specific 3D biventricular heart models [8]. Deep learning-based approaches have been increasingly used in recent times for cardiac mesh reconstruction from cine MR slices. In [9], the problem of mesh fitting from sparse inputs was transformed into a 3D volumetric inpainting problem followed by isosurfacing from dense volumetric data, while the geometric deep learning method was utilized in [10] to reconstruct the biventricular anatomy point clouds.

Although there exist few research works that addressed the problem of 3D reconstruction from 2D cine MR slices, the existing methods only focused on the reconstruction of the two ventricles and did not consider the atria in the 3D models. The underlying reason is that the atria are visible only from a very limited number of image planes, typically 3-4 for the left atrium and 1-3 for the right atrium, in the clinically used 2D cine MR acquisitions. The automated reconstruction of 3D whole-heart meshes has high clinical importance, including in biomedical simulations and multimodal integration, specifically for the localization of coronary vascular structures on 3D heart surface. In this regard, the objective

*Research supported by the British Heart Foundation and the CompBioMed 2 Centre of Excellence in Computational Biomedicine (European Commission Horizon 2020 research and innovation programme).

[1]A. Banerjee is with the Division of Cardiovascular Medicine, Radcliffe Department of Medicine, University of Oxford, Oxford OX3 9DU, UK and also with the Institute of Biomedical Engineering, Department of Engineering Science, University of Oxford, Oxford OX3 7DQ, UK (corresponding author) abhirup.banerjee@cardiov.ox.ac.uk

[2]E. Zacur and V. Grau are with the Institute of Biomedical Engineering, Department of Engineering Science, University of Oxford, Oxford OX3 7DQ, UK vicente.grau@eng.ox.ac.uk

[3]R. P. Choudhury is with the Division of Cardiovascular Medicine, Radcliffe Department of Medicine, University of Oxford, Oxford OX3 9DU, UK robin.choudhury@cardiov.ox.ac.uk

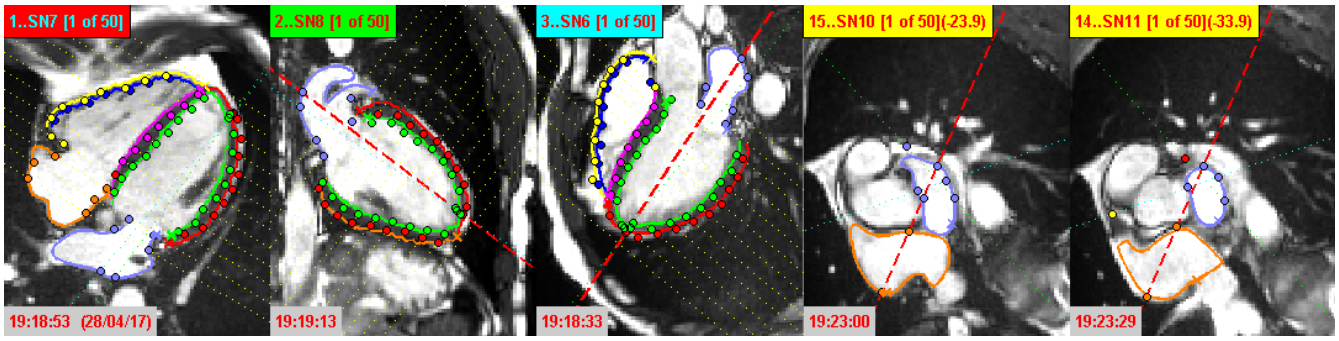

Fig. 1. From left to right: HLA view, VLA view, LVOT view, and two SAX slices. The green, blue, red, yellow, pink, indigo, and orange contours respectively denote the LV and RV endocardial contours, LV and RV epicardial contours, septal wall, and the LA and RA endocardial contours on 2D cine MR slices. The coloured dots represent the position of corresponding contours on the intersecting slice.

of the current work is to develop an automated method for 3D whole-heart mesh reconstruction, including both atria and both ventricles, from clinically available 2D cine CMR scans. In order to mitigate the data sparsity due to limited number of slices, we have first optimally fitted a statistical shape model (SSM), generated from high-resolution multislice computed tomography (CT) images, to the extracted heart contours in 3D space. The initial reconstructed mesh is deformed to minimize the surface to contours distances in order to accommodate the patient-specific variation in the 3D cardiac anatomy. The performance of the proposed reconstruction method is evaluated on a cohort of 30 subjects randomly selected from the UK Biobank study [11]. The proposed approach has been able to produce high-quality 3D whole-heart meshes with average contours to surface distance less than the underlying image resolution, and with volumetric clinical metrics estimated from the 3D model within acceptable ranges reported in the previous literature.

II. METHODS

This section presents the proposed approach for 3D whole-heart mesh reconstruction. The method starts with automated extraction of the heart contours and the 3D biventricular mesh reconstruction. The SSM is then optimally fitted to the sparse heart representation to generate the initial 3D whole-heart mesh. The initial mesh is iteratively deformed to the heart contours in 3D space to generate the final patient-specific 3D whole-heart mesh.

A. Preprocessing and Biventricular Reconstruction

The initial preprocessing step of our method has been performed using the automated pipeline presented in [8]. Given the acquired CMR image files as the only input, the pipeline starts by automatically selecting the long axis (LAX) and short axis (SAX) cardiac slices generated by standard cine CMR studies. The CMR slices for the standard cine protocol are three LAX views, namely the horizontal long axis (HLA) (Fig. 1(a)), vertical long axis (VLA) (Fig. 1(b)), and left ventricular outflow tract (LVOT) (Fig. 1(c)), and the stack of short axis (SAX) views (Fig. 1(d)-(e)). In order to identify the epicardial, left ventricle (LV) and right ventricle (RV) endocardial, and left atrium (LA) and right atrium (RA) endocardial contours from all 2D cine CMR slices, we have automatically segmented the heart slices in 6 classes, namely, LV cavity, LV myocardium, RV cavity, LA cavity, RA cavity, and background. The deep learning based method proposed by Bai et al. [12] has been employed in this step, since it has been shown to segment heart structures from cine MR slices with human-level accuracy. Since at this time we do not have any pre-trained network for the LVOT slices, we have manually contoured the LV, RV, and LA endocardial and LV epicardial surfaces on the LVOT slices. The SAX stack often includes 1-2 SAX images of heart structures over the basal plane (Fig. 1(d)-(e)), which are also manually contoured.

Automated methods are applied to remove both in-plane [13] and out-of-plane [14] misalignments between slices, due to the breathing, heart-beating, or subject movements. The 3D biventricular surface is then reconstructed by maximising fitting to LV and RV endocardial and epicardial contours, while maintaining the optimal interpolation characteristics.

It should be noted here that the proposed approach can reconstruct patient-specific 3D whole-heart meshes without an initial 3D biventricular reconstruction. However, due to the limited amount of information on atrial structures as compared to the ventricular structures from the available 2D cine CMR scans, we prefer to resample along the whole biventricular surface as our initial sparse representation, instead of utilizing only the LV and RV endocardial and epicardial contours along the cine CMR planes. Figure 2(a) presents the sparse representation of the whole-heart after misalignment correction, along with the reconstructed biventricular surfaces.

B. Fitting the Statistical Shape Model

In the clinically available 2D cine MR slices, the LA is usually visible on all three LAX slices, namely the HLA, VLA, and LVOT, and sometime on 1-2 SAX slices acquired over the basal plane. The RA, on the other hand, is visible only on the HLA slice and often on 1-3 SAX slices. Hence, in order to generate the heart atrial meshes from the available sparse and limited information, we have employed a high-resolution statistical shape model (SSM) of the whole human heart [15] for our initial 3D whole-heart mesh reconstruction. The SSM was generated from the 3D computed tomography (CT) scans of a clinical cohort of 134 subjects that underwent a CT examination as part of their routine diagnostic protocol

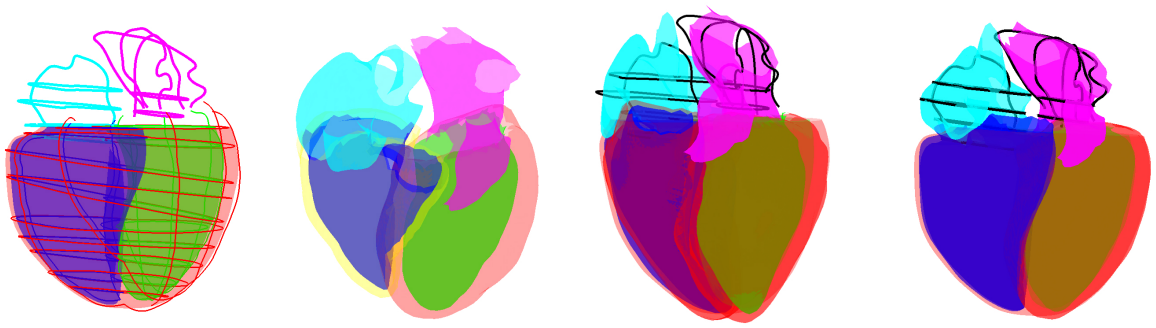

Fig. 2. (a) Sparse 3D contours after misalignment correction, including the initial 3D biventricular surface; (b) the mean SSM; (c) optimally fitted SSM over sparse representation; and (d) the final patient-specific reconstructed 3D whole-heart mesh after iterative deformation. The green, blue, red, magenta, and cyan surfaces respectively denote the LV and RV endocardium, epicardium, and the LA and RA endocardial surfaces.

for suspected coronary artery disease, and follow-up. After applying a series of global registration, diffeomorphic non-rigid registration, and deformation over the 3D heart scans, the principal component analysis was applied to build the final SSM. The 50 principal modes of variation accounts for 90% of variance in the dataset. The model contains non-manifold meshes of 13 cardiac components and coronary arteries, including both atria, both ventricles, septum, aorta, and left and right coronary arteries.

In order to approximately align the input sparse heart representation with the SSM, the proposed method first extracts three fiducial landmarks, namely the center of the LV endocardium at base, center of the RV endocardium at base, and apical point of the LV on the sparse model. The corresponding three landmarks are automatically identified on the SSM, and the sparse model is registered to the SSM following rigid transformation. Next, the LV and RV endocardial, LV and RV epicardial, and LA and RA endocardial surfaces are automatically extracted from the SSM and the meshes are fitted to the corresponding sparse heart representation in 3D space by the optimal estimation of principal components of the SSM, followed by rigid transformation, such that:

$$\min_{b,\psi} \sum_{k} \sum_{i} d(C_i^k, \psi(\bar{X} + \Phi b))^2, \tag{1}$$

where C_i^k is the ith point on kth cardiac structure, $\bar{X}$ the mean shape model, $\Phi = (\phi_1, \phi_2, \cdots)$ the SSM modes of variations, b the estimated set of parameters along the principal modes, and ψ the rigid transformation. The optimally fitted SSM over the sparse heart contours of Fig. 2(a) is presented in Fig. 2(c).

C. Deforming for patient-specific mesh reconstruction

The initial whole-heart mesh generated by optimal fitting of the SSM is inherently limited by the overall variability in the input cohort and hence, they cannot accurately capture the patient-specific anatomical variations. To address this issue, a deformation step is applied on the 3D reconstructed mesh to minimize the distance to the sparse representation while ensuring the smoothness and local topoligical properties [16]. The deformation field is first computed by considering the closest point from each of the 'attractor' points on the sparse model to the initial 3D mesh. The points on the mesh are then pulled towards the corresponding attractor points, and this deformation is extrapolated via the use of approximating thin plate splines (TPS) [17]. The process is iteratively applied in small consecutive steps, to ensure small, smooth deformations. Let F be the deformation field such that

$$\arg\min_{F} \lambda \sum_{i} (||F(P_i) - Q_i'||)^2 + J_2^3(F) \tag{2}$$

$$\text{and} \quad Q_i' = P_i + \beta \frac{(Q_i - P_i)}{||Q_i - P_i||} \tag{3}$$

where $\{P_i\}$ is the set of closest points on the surface M_t to the attractor points $\{Q_i\}$ on sparse model and J_2^3 is the TPS functional using derivatives of order 2 and image dimensions 3. The deformation $M_{t+1} = F(M_t)$ is iteratively applied in a diffeomorphic manner, resulting in a composition of several smooth approximations approaching initial mesh M towards the sparse representation. Laplacian smoothing, decimation, and affine transformation are applied in the end to ensure the local geometric and topological characteristics of the final reconstructed mesh (Fig. 2(d)).

III. RESULTS

In order to evaluate the performance of the proposed 3D whole-heart reconstruction approach, we have randomly selected a heterogeneous cohort of 30 subjects (15 female and 15 male) from the UK Biobank study [11]. The dataset includes an HLA, a VLA, an LVOT, and a stack of SAX cine MR slices for each subject. The number of SAX cardiac cine MR slices varies between 8 to 13. The images have in-plane resolution of 1.8269 mm and the distance between SAX slices is 10 mm. For each subject, the frame number 1 is selected as the end-diastolic frame in our analysis. A random sample of four reconstructed 3D whole-heart meshes is presented in Fig. 3.

A. Evaluation of Reconstruction Quality

In order to quantitatively evaluate the performance of 3D reconstructed meshes, we have measured the distances of the 3D reconstructed cardiac substructures from their

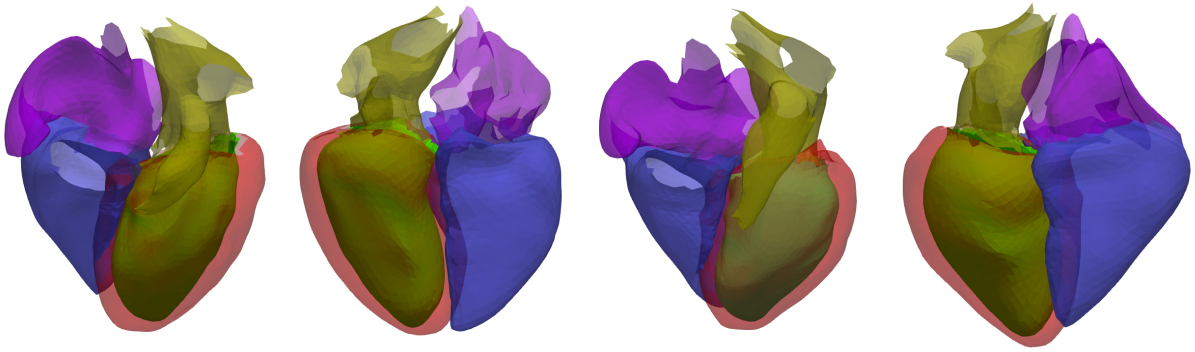

Fig. 3. An example of four reconstructed 3D whole-heart meshes. (a) and (c) anterior views; (b) and (d) posterior views. The green, blue, red, moss, and purple surfaces respectively denote the LV and RV endocardium, LV epicardium, and the LA and RA endocardium.

TABLE I

RECONSTRUCTION PERFORMANCE IN TERMS OF AVERAGE SURFACE TO CONTOURS DISTANCE

Cardiac structure	Female	Male
LV endocardium	0.538 $\pm$ 0.183	0.573 $\pm$ 0.121
RV endocardium	0.745 $\pm$ 0.162	0.778 $\pm$ 0.138
Epicardium	0.981 $\pm$ 0.289	1.068 $\pm$ 0.206
LA endocardium	0.424 $\pm$ 0.373	0.419 $\pm$ 0.138
RA endocardium	0.321 $\pm$ 0.273	0.383 $\pm$ 0.164

Values represent mean $\pm$ standard deviation.

input sparse representations. In our dataset of 30 subjects, the distances for the LV endocardium, RV endocardium, epicardium, LA endocardium, and RA endocardium are measured as 0.556 $\pm$ 0.147, 0.761 $\pm$ 0.143, 1.025 $\pm$ 0.241, 0.421 $\pm$ 0.265, and 0.352 $\pm$ 0.215 mm, respectively. There's no statistically significant difference between the reconstruction performance on female and male subjects, and in all cases the distances are well within the underlying image pixel resolution. The quantitative results are separately presented in Table I for female and male subjects.

TABLE II

ESTIMATED 3D VOLUMETRIC CLINICAL METRICS

Sex	Clinical Metric	Proposed	Benchmark [18]
Female	LVEDV (ml)	112.60 $\pm$ 14.08	124 $\pm$ 21
	RVEDV (ml)	135.54 $\pm$ 14.22	130 $\pm$ 24
	LAEDV (ml)	42.65 $\pm$ 9.63	62 $\pm$ 17 (maximal)
	RAEDV (ml)	45.14 $\pm$ 8.84	69 $\pm$ 17 (maximal)
Male	LVEDV (ml)	149.25 $\pm$ 22.84	166 $\pm$ 32
	RVEDV (ml)	177.34 $\pm$ 35.04	182 $\pm$ 36
	LAEDV (ml)	69.92 $\pm$ 50.39	71 $\pm$ 19 (maximal)
	RAEDV (ml)	67.36 $\pm$ 22.83	93 $\pm$ 27 (maximal)

Values represent mean $\pm$ standard deviation.

B. Estimation of 3D Volumetric Clinical Metrics

In order to evaluate the clinical application of the reconstructed meshes, common volumetric clinical metrics, namely the LV end-diastolic volume (LVEDV), RV end-diastolic volume (RVEDV), LA end-diastolic volume (LAEDV), and RA end-diastolic volume (RAEDV), are computed. Results are presented separately for female and male subjects in Table II, along with corresponding values reported in the benchmark study of Petersen et al. [18].

Overall, we observe that our 3D reconstructed meshes achieve plausible scores for all analyzed metrics and is able to accurately capture sex-related differences. This is shown by the higher left and right ventricular volumes reported for male cases compared to the female ones, also present in the benchmark study. Since we have randomly selected 30 subjects (15 in each group) with varying demography in our current work, the estimated volumetric metrics demonstrate higher variability, as compared to the benchmark study over 432 female and 368 male subjects. However, they are still within the acceptable ranges from the reported literature. The study of [18] considered the maximal atrial volumes in only the HLA and VLA acquisition planes and hence, those results are not comparable with our estimated LAEDV and RAEDV.

IV. DISCUSSION

Patient-specific 3D whole-heart mesh reconstruction is quintessential for numerous modelling and simulation-based applications, such as the digital twin [19] and in-silico clinical trials [20], that account for the effect of anatomical variability in the human population. In this regard, our proposed approach has enabled the combined reconstruction of high-quality 3D atrial and ventricular meshes from a limited number of clinically acquired cine CMR scans. The geometric accuracy of the reconstructed meshes are verified using the average surface to input contours distance, which is well below the underlying image resolution. The clinical accuracy of the reconstructed meshes are evaluated over estimated common volumetric metrics, which are within acceptable ranges from the reported literature. The high variability in the estimated volumetric measures indices that the proposed approach can capture high anatomical variability in the human population due to its final deformation step and can be applicable even on diseased subjects.

One of the biggest advantages of the proposed approach is that it can be applied over any number of input image planes. Although our aim was to develop an approach based on very limited number of image scans from standard clinical cine CMR protocol, the proposed approach will be applicable when additional higher number of image scans in LAX view or in SAX view for atrial structures will be available. Although in this work we have only demonstrated the performance of 3D whole-heart mesh reconstruction at the end-diastolic phase, the proposed approach can be applied at any phase in the cardiac cycle.

V. CONCLUSIONS

In this paper, we have presented a novel approach for automated patient-specific 3D whole-heart mesh reconstruction from clinically available 2D cine CMR scans. The reconstructed high-quality meshes are well suited for numerous clinical and research applications including biomedical simulations, virtual surgery, treatment planning, and integration of multimodal information such as the multimodal CMR, CT, and most interestingly, the coronary vasculatures.

ACKNOWLEDGMENT

This research has been conducted using the UK Biobank Resource under Application Number '40161'. The authors express no conflict of interest. The work of A. Banerjee was supported by the British Heart Foundation (BHF) Project under Grant HSR01230. The work of V. Grau was supported by the CompBioMed 2 Centre of Excellence in Computational Biomedicine (European Commission Horizon 2020 research and innovation programme, grant agreement No. 823712). The authors acknowledge the use of services and facilities of the Institute of Biomedical Engineering, University of Oxford, United Kingdom.

REFERENCES

[1] E. Dall'Armellina, T. D. Karamitsos, S. Neubauer, and R. P. Choudhury, "CMR for characterization of the myocardium in acute coronary syndromes," *Nature Reviews Cardiology*, vol. 7, no. 11, pp. 624–636, 2010.

[2] A. Khatamian and H. R. Arabnia, "Survey on 3D surface reconstruction," *Journal of Information Processing Systems*, vol. 12, no. 3, pp. 338–357, 2016.

[3] L. Liu, C. Bajaj, J. O. Deasy, D. A. Low, and T. Ju, "Surface reconstruction from non-parallel curve networks," *Computer Graphics Forum*, vol. 27, no. 2, pp. 155–163, 2008.

[4] Z. Huang, M. Zou, N. Carr, and T. Ju, "Topology-controlled reconstruction of multi-labelled domains from cross-sections," *ACM Transactions on Graphics*, vol. 36, no. 4, pp. 1–12, 2017.

[5] M. Zou, M. Holloway, N. Carr, and T. Ju, "Topology-constrained surface reconstruction from cross-sections," *ACM Transactions on Graphics*, vol. 34, no. 4, pp. 1–10, 2015.

[6] Z. Zhang, K. Konno, and Y. Tokuyama, "3D terrain reconstruction based on contours," in *9th International Conference on Computer Aided Design and Computer Graphics*, 2005, pp. 1–6.

[7] Z. Wang, N. Geng, and Z. Zhang, "Surface mesh reconstruction based on contours," in *International Conference on Computational Intelligence and Software Engineering*, 2009, pp. 1–4.

[8] A. Banerjee, J. Camps, E. Zacur, C. M. Andrews, Y. Rudy, R. P. Choudhury, B. Rodriguez, and V. Grau, "A completely automated pipeline for 3D reconstruction of human heart from 2D cine magnetic resonance slices," *Philosophical Transactions of the Royal Society A: Mathematical, Physical and Engineering Sciences*, vol. 379, no. 2212, p. 20200257, 2021.

[9] H. Xu, E. Zacur, J. E. Schneider, and V. Grau, "Ventricle surface reconstruction from cardiac MR slices using deep learning," in *International Conference on Functional Imaging and Modeling of the Heart*, 2019, pp. 342–351.

[10] M. Beetz, A. Banerjee, and V. Grau, "Biventricular surface reconstruction from cine MRI contours using point completion networks," in *2021 IEEE 18th International Symposium on Biomedical Imaging (ISBI)*, 2021, pp. 105–109.

[11] S. E. Petersen, P. M. Matthews, F. Bamberg, D. A. Bluemke *et al.*, "Imaging in population science: cardiovascular magnetic resonance in 100,000 participants of UK Biobank - rationale, challenges and approaches," *Journal of Cardiovascular Magnetic Resonance*, vol. 15, no. 46, pp. 1–10, 2013.

[12] W. Bai, M. Sinclair, G. Tarroni, O. Oktay *et al.*, "Automated cardiovascular magnetic resonance image analysis with fully convolutional networks," *Journal of Cardiovascular Magnetic Resonance*, vol. 20, no. 65, pp. 1–12, 2018.

[13] B. Villard, E. Zacur, E. Dall'Armellina, and V. Grau, "Correction of slice misalignment in multi-breath-hold cardiac MRI scans," in *Statistical Atlases and Computational Models of the Heart. Imaging and Modelling Challenges*, 2017, pp. 30–38.

[14] A. Banerjee, E. Zacur, R. P. Choudhury, and V. Grau, "Optimised misalignment correction from cine MR slices using statistical shape model," in *Medical Image Understanding and Analysis*, 2021, pp. 201–209.

[15] C. Hoogendoorn, N. Duchateau, D. Sanchez-Quintana, T. Whitmarsh, F. M. Sukno, M. De Craene, K. Lekadir, and A. F. Frangi, "A high-resolution atlas and statistical model of the human heart from multislice CT," *IEEE Transactions on Medical Imaging*, vol. 32, no. 1, pp. 28–44, 2013.

[16] B. Villard, V. Grau, and E. Zacur, "Surface mesh reconstruction from cardiac MRI contours," *Journal of Imaging*, vol. 4, no. 1, pp. 1–21, 2018.

[17] K. Rohr, H. S. Stiehl, R. Sprengel, T. M. Buzug, J. Weese, and M. H. Kuhn, "Landmark-based elastic registration using approximating thin-plate splines," *IEEE Transactions on Medical Imaging*, vol. 20, no. 6, pp. 526–534, 2001.

[18] S. E. Petersen, N. Aung, M. M. Sanghvi, F. Zemrak *et al.*, "Reference ranges for cardiac structure and function using cardiovascular magnetic resonance (CMR) in Caucasians from the UK Biobank population cohort," *Journal of Cardiovascular Magnetic Resonance*, vol. 19, no. 18, pp. 1–19, 2017.

[19] J. Corral-Acero, F. Margara, M. Marciniak, C. Rodero *et al.*, "The 'Digital Twin' to enable the vision of precision cardiology," *European Heart Journal*, vol. 41, no. 48, pp. 4556–4564, 2020.

[20] B. Rodriguez, "The 18th FRAME annual lecture, October 2019: Human in silico trials in pharmacology," *Alternatives to Laboratory Animals*, vol. 47, no. 5-6, pp. 221–227, 2019.